Visualization of Radiation-Pattern Characteristics of Phased Arrays Using Digital Phase Shifters

M. Clénet and G. A. Morin

Defence R&D Canada – Ottawa
Ottawa, Ontario, K1A 0Z4, Canada
Tel: +1 (613) 993-7397; Fax: +1 (613) 998-4560;
E-mail: michel.clenet@drdc-rddc.gc.ca; gilbert.morin@ddrdc-rddc.gc.ca

Abstract

This article presents graphical investigations of the array factor of phased arrays with digital phase shifters. A software program, based on basic antenna array theory, has been developed in *MATLAB* to obtain the main array characteristics (array factor and directivity). The array factors of linear arrays of different sizes with different types of phase shifters have been studied as a function of the number of bits and the frequency. Unconventional two-dimensional color graphical representations are used to identify some characteristics of the array factor of arrays with digital phase shifters that can not be so clearly and quickly visualized with conventional graphical representations. In particular, the effects of quantization on the array factor for arrays of different sizes and for phase shifters with different numbers of bits, over scanning, and frequency ranges, are shown using this representation. Numerous data are also provided.

Keywords: Antenna arrays; antenna radiation patterns; beam steering; delay lines; graphics; linear arrays; phased arrays; phase shifters; quantization

1. Introduction

Phased-array antennas have now been studied for about 70 years [1]. First built for military radar applications, they received much more attention during the last two decades because of the extent of their utilization in communication systems, especially mobile and satellite communications. Cost is a key issue for commercial as well as military applications, and much on-going research is devoted to developing T/R [transmitter/receiver] modules, phase shifters, and time-delay units with good characteristics under this constraint. A step forward has been achieved at the end of the century with advances in technology like MMIC (monolithic microwave integrated circuits) and MEMS (micro-electromechanical systems). In addition to lowering the cost, high integration is obtained, reducing the size of the devices.

Consequently, digital phase shifters became preferred for such applications. The size of the phase shifter can be significant, and is directly related to the number of bits, which is an important factor for the radiation performance of the array. Digital phase shifters deliver an approximated phase to each element to steer the beam in the desired direction. The accuracy of this approximation depends on the number of phase-shifter bits. Patterns produced by arrays with digital phase shifters exhibit high-level sidelobes and a reduction in directivity. To analyze the effect of phase quantization, studies on phased-array antennas using digital phase shifters were carried out, and are reported in this paper.

A software program has been developed in *MATLAB* to carry out this study [2]. This program, called *PAASoM* – standing for "Phased array antenna software in *MATLAB*" – is based on basic array-antenna theory. Although the results presented here are limited to linear phased arrays, the code is able to compute arrays of different geometries (linear, rectangular, triangular, hexagonal, octagonal, circular, or others), and with different regular or irregular lattices (rectangular or triangular). Constant-phase phase shifters and switched-line phase shifters, analog or digital with different numbers of bits, can be associated with each element, as well as true-time-delay feed systems. Amplitude weightings are also possible, considering the usual distributions (power of cosine with or without pedestal, Taylor, Dolph-Chebychev, and others [3]). The results can be visualized with conventional two-dimensional graphs, or with an unconventional two-dimensional color representation. The latter has been previously used by many authors for fixed-beam antennas to show their radiation patterns over half-space, as in [4] and [5], for example. This representation is helpful to clearly and quickly visualize some radiation characteristics of phased arrays over an operating range.

The first part of the study considers the effect of the number of phase-shifter bits, as the radiation performance of the arrays depends strongly on this parameter. The investigations concern linear arrays with different numbers of elements, controlled by digital phase shifters with different numbers of bits. For comparison purposes, the results of these arrays incorporating analog phase

DREO SL 2001-102

106-03561/

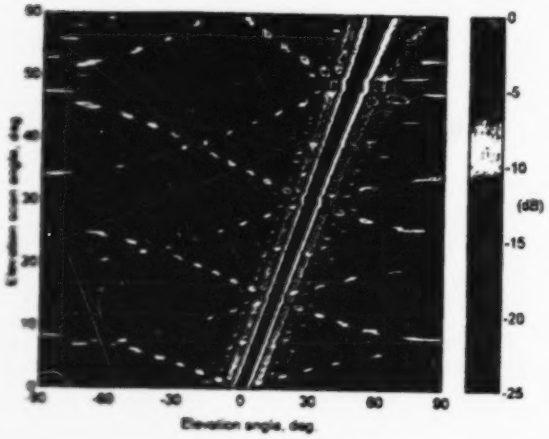

Figure 1a. The two-dimensional color Cartesian of the array factor of a 25-element linear array using three-bit phase shifters, with the scan angle as a parameter.

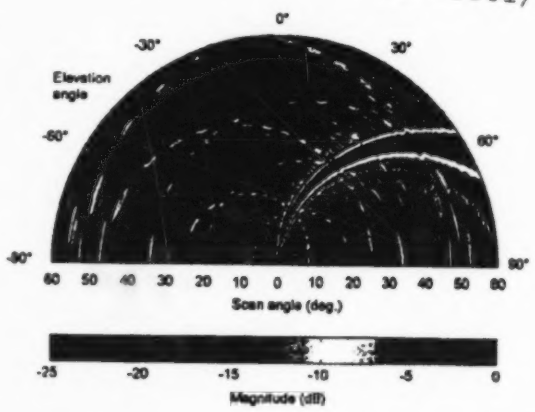

Figure 1b. The two-dimensional color polar representation of the array factor of a 25-element linear array using three-bit phase shifters, with the scan angle as a parameter.

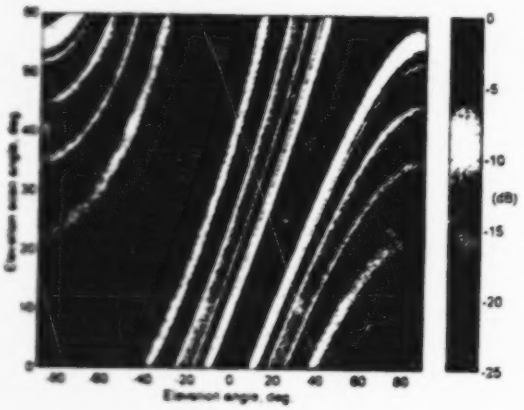

Figure 3. The array factor of an eight-element linear array with analog phase shifters as a function of scan angle (color scale in dB).

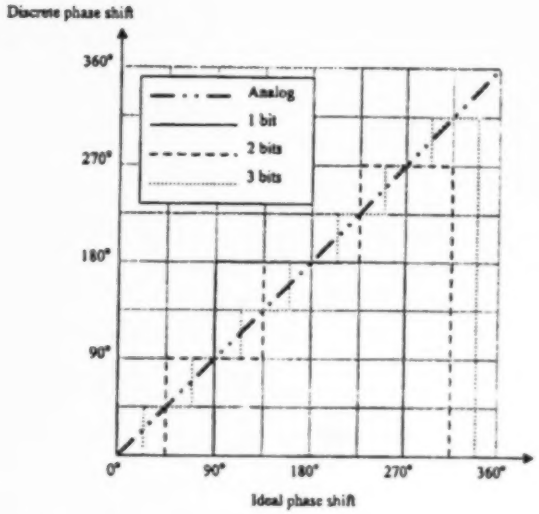

Figure 4. The discrete phase values of the phase shifter for different numbers of bits.

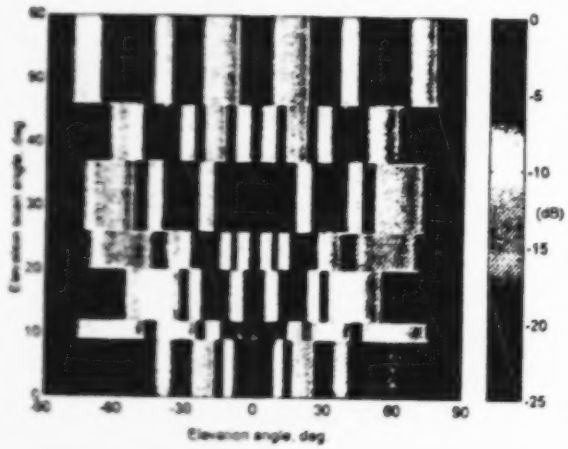

Figure 5. The array factor of an eight-element linear array with one-bit phase shifter as a function of scan angle (color scale in dB).

29530

shifters are also presented. By definition, an analog phase shifter is a phase shifter that can deliver the exact phase to any array element of a phased array, to steer the beam in the desired direction for a given frequency.

The second part of this study presents the results of the array-factor characteristics as a function of frequency. A 64-element array is considered, fed by analog and digital phase shifters. Arrays with constant-phase and switched-line phase shifters are compared to arrays using true-time-delay lines. Results of an array with switched-line phase shifters for each element and true-time delay units at sub-array levels are also reported. This analysis clearly underlines advantages and drawbacks of each technique used to control phased-array scanning.

Before presenting these results, the graphical representation used throughout this paper will be introduced.

2. Graphical Representations

Conventionally, radiation patterns are represented in two dimensions (2D), in Cartesian or polar coordinate systems. In the Cartesian coordinate system, the magnitude of the radiated field, usually in decibels (dB), is indicated on the Y axis, whereas the angular parameter, commonly the elevation angle, θ, is on the X axis. Sometimes, the angular parameter is replaced with the quantity $u = \sin\theta$ or $u = \sin\theta\cos\varphi$, depending on the context. In the polar coordinate system, the radius usually represents the magnitude of the radiated field, and the angle represents the angular parameter. When comparison is required, several curves are plotted on the same graph. Different line types or colors are then used to distinguish among them. Sometimes, another dimension is added to represent the pattern variation as a function of a parameter, such as the azimuth angle, the frequency, or others. The third dimension can be either another axis or the color parameter. The data are then represented in three dimensions (3D) or two-dimensional color plots.

In the case of a three-dimensional representation, the magnitude of the radiated field is indicated, usually in dB, on the Z axis, whereas the X and Y axes show the elevation and azimuth angles, or the quantities $u = \sin\theta\cos\varphi$ and $v = \cos\theta\cos\varphi$, varying between $[-1;1]$. Such a representation gives a general overview of the radiation performance of the antenna. However, as the three-dimensional representation is actually two-dimensional on a planar surface, paper, or monitor screen, quantitative data are not easily extracted. In the case of a two-dimensional color representation in a Cartesian coordinate system, a color scale represents the magnitude of the radiated power, whereas the two-dimensional coordinates represent either (θ,φ) or (u,v). A combination of both three dimensions and color is also used, giving more legibility to the graphical representation. The parameters can also be other than elevation and azimuth angles, depending on the user's interest. In phased-array antennas, for instance, one parameter of interest is the scan angle.

An attractive representation is then the two-dimensional color plot, where, in the Cartesian coordinate system, the X axis represents the elevation angle and the Y axis represents the scan angle (Figure 1a). A polar coordinate system is sometimes preferred, with the radius representing the scan angle and the angular value the elevation angle (Figure 1b). The choice of the coordinate system depends mostly on the characteristics we focus on, and the considered parameter. For example, the Cartesian coordinate system is better suited when the scan angle is the parameter, while the polar plot is better suited when the frequency is the parameter of interest, as will be shown in Section 4.

Throughout this paper, the two-dimensional color representation will be used to show radiation patterns of phased arrays using digital phase shifters, over either scan angle or a frequency range. Such a representation is helpful in identifying some characteristics of the array factor of a phased array that cannot be so clearly and quickly visualized with conventional two-dimensional plots.

3. Quantization Effects on Radiation Patterns of Linear Arrays with Elements Fed through Digital Phase Shifters

This section examines the effect on the directivity and array-factor characteristics of linear phased arrays for different numbers of phase-shifter bits. The results for arrays with different numbers of elements are reported and analyzed. For each array, phase shifters with two to five bits are considered. Two cases are fully described: an eight-element array and a 64-element array. Other arrays were investigated (from eight to 128 elements), but only summarized data are reported, as the results were similar to those of the detailed studies.

3.1. Array Configuration

The array configuration is shown in Figure 2. The elements, which are point sources, were positioned on the horizontal axis. The inter-element spacing (d) is chosen to be half a wavelength, to avoid grating lobes in the half space above the ground. The phase of the phase shifter for each element was chosen to be the closest one to the ideal phase to steer the main beam in the desired direction. As the study was for a single frequency, the type of phase shifter did not matter.

The array factors presented in this section are calculated for $-90° \le \theta \le 90°$ with a 0.2° step, and for $0° \le \theta_0 \le 60°$ with a 0.2° step, unless otherwise noted. θ is the elevation angle, and θ_0 is the elevation scan or steering angle. In addition, some average results over a scanning range are given to quantify array-factor characteristics, such as scan-angle deviation, sidelobe level, or

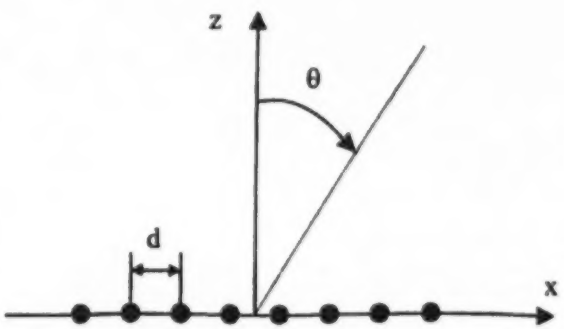

Figure 2. The linear array configuration.

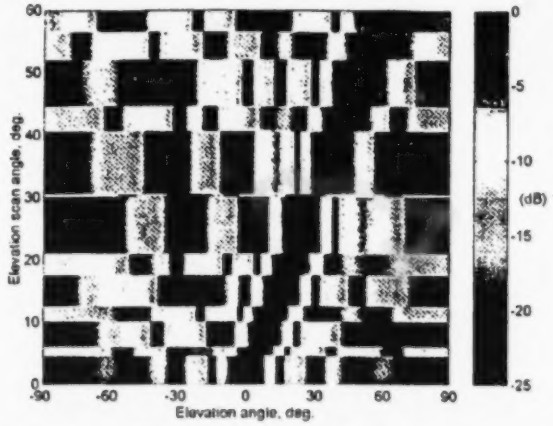

Figure 6. The array factor of an eight-element linear array with two-bit phase shifters as a function of scan angle (color scale in dB).

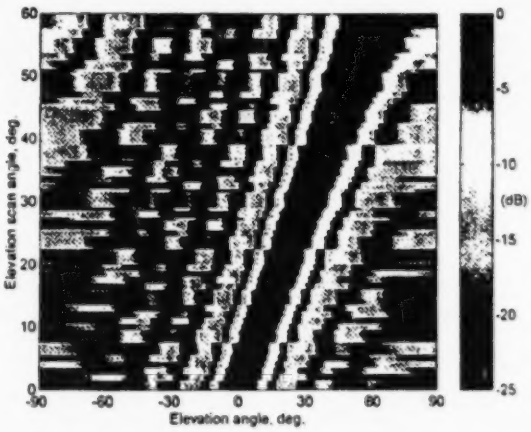

Figure 8. The array factor of an eight-element linear array with four-bit phase shifters as a function of scan angle (color scale in dB).

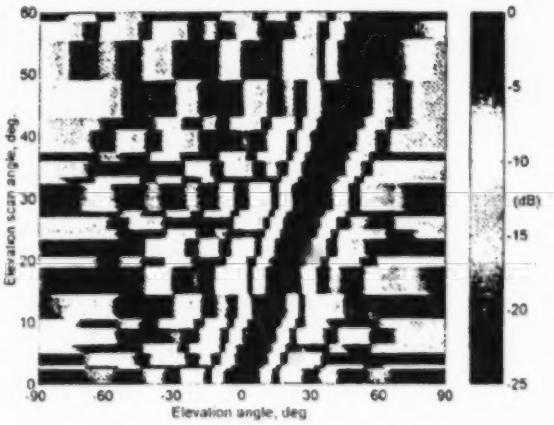

Figure 7. The array factor of an eight-element linear array with three-bit phase shifters as a function of scan angle (color scale in dB).

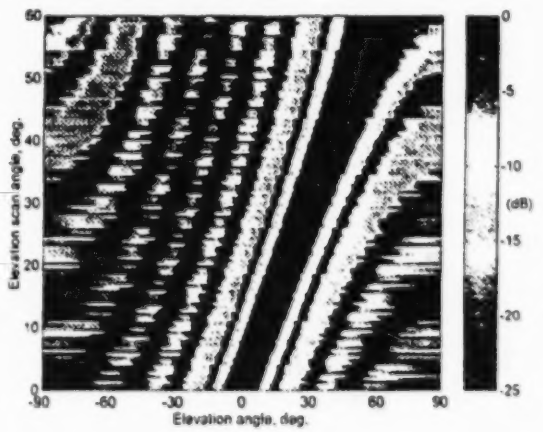

Figure 9. The array factor of an eight-element linear array with five-bit phase shifters as a function of scan angle (color scale in dB).

directivity loss. Unless otherwise noted, the average results mentioned in this section were calculated for $0° \le \theta_0 \le 60°$ with a 1° step.

3.2. Eight-Element Array

In order to estimate the discrepancies of the array factor characteristics due to the use of digital phase shifters, the array-factor characteristics of an eight-element phased array with analog phase shifters are first summarized. For the case of analog phase shifters, each element was given the precise phase to scan in the θ_0 direction.

Figure 3 gives a two-dimensional color representation of array factors. As mentioned in the previous section, the graph shows the power of the radiated field for an elevation scan angle from 0° to 60° on the vertical axis, and the elevation angle from −90° to 90° on the horizontal axis. For each elevation scan angle chosen (depicted on the vertical axis), the horizontal line through that value gives a plot of the array factor as a function of the elevation angle, with the magnitude of the array factor given by its color. In such a representation, it is easy to visualize the main lobe, sidelobes, nulls, and half-power-beamwidth variations when the scan angle changes. Particularly, with the help of the black contour line at the −3 dB level, one can notice the widening of the half-power beamwidth (HPBW) with the increase in the scan angle. In the broadside direction, the HPBW is 12.8°, and it slowly increases to reach 16.9° for $\theta_0 = 40°$ and 28.9° for $\theta_0 = 60°$. The maximum sidelobe level (max. SLL) is constant over the scanning range, and equals −12.8 dB. The levels of the second and third sidelobes are −16.5 dB and −17.9 dB, respectively. Also, the level of the grating lobe, visible in the top left corner of the figure, is higher than −10 dB for scan angles above 54°, and reaches −4.3 dB for $\theta_0 = 60°$.

3.2.1 One-Bit Phase Shifter

With a one-bit phase shifter, the phase is limited to two states: 0° and 180° (Figure 4). The maximum deviation from the phase that is required for each element to steer the beam in the desired direction is then 90°. This configuration leads to a significant scan-angle discrepancy. In addition, two simultaneous main lobes are generated, as only two phase states are possible (0° and 180°). In other words, the array is not able to distinguish the left or the right sides. The additional main lobe is called a quantization lobe, and will be discussed in Section 3.3.

Figure 5 shows the two-dimensional color plot of the array factor in the main plane for a scan angle from 0° to 60° with 1° increments. The effect of phase quantization appears clearly. The black line from (0,0) to (60,60) indicates the theoretical position of the array-factor maximum for the desired scan angle.

Only seven phase distributions are available to cover the 60° scan range. From $\theta_0 = 0°$ to 9°, all the elements are in phase. Then, with the exception of those elements at the center of the array, the phase of the elements changes as the scan angle changes. Since the phase reference is at the array center, the phase distribution of the array is symmetric about the center line of the array. The various phase distributions are detailed in Table 1. Note that the maximum power can not be reached for $\theta_0 > 9°$ because of the presence of two main lobes located symmetrically with respect to the broadside direction.

Table 1. The phase of the input of each element from 0° to 60° scan angle (radians).

	Element Number							
Scan Angles	1	2	3	4	5	6	7	8
1: 0° to 9°	0	0	0	0	0	0	0	0
2: 9° to 12°	π	0	0	0	0	0	0	π
3: 12° to 20°	π	π	0	0	0	0	π	π
4: 20° to 26°	π	π	π	0	0	π	π	π
5: 26° to 37°	0	π	π	0	0	π	π	0
6: 37° to 46°	0	0	π	0	0	π	0	0
7: 46° to 60°	π	0	π	0	0	π	0	π

3.2.2 Two-Bit Phase Shifter

A two-bit phase shifter provides four possible phase states: 0°, 90°, 180°, and 270° (Figure 4). The maximum deviation from the phase that is required for each element to steer the beam in the desired direction is then 45°. The number of phase distributions in the 60° scan-angle range increases compared to the previous case, as shown in Figure 6.

The scan-angle deviation is high for several steering angles. The array factor obtained does not change for scan angles from 21° to 30° (the scan angle obtained is 25.4°), and another phase distribution gives the same pattern for a desired scan angle from 30.5° to 40.5° (the scan angle obtained is 36.5°).

The signals radiated by each element are not optimally combined in the far field due to the limited number of phase states, and therefore the result is that the sidelobes do not appear at the same position and with the same power. Thus, the maximum sidelobe level (SLL) is increased. As an example, the maximum sidelobe level is −5.8 dB for $21° \le \theta_0 \le 40°$, excluding θ_0 near 30°. For $0° \le \theta_0 \le 60°$, the maximum sidelobe level fluctuates between −5.7 dB and −12.8 dB, and the average maximum sidelobe level is −6.97 dB. This leads to a 0.8 dB average drop of the maximum directivity, with a 1.63 dB maximum drop for $\theta_0 = 30°$.

3.2.3 Three-Bit Phase Shifter

A three-bit phase shifter gives eight possible phase states, starting at 0° with a 45° step (Figure 4). The maximum deviation of the phase of each element is then 22.5°. The scan-angle error is considerably reduced compared to the case with the two-bit phase shifter, as shown in Figure 7.

The patterns remain constant in the largest angular range for $43° \le \theta_0 < 49°$, and for $49° \le \theta_0 < 55.5°$. The maximum deviation of 3.9° occurs for $\theta_0 = 49°$, while the average scan-angle deviation over the scanning range, calculated for $0° \le \theta_0 < 60°$ with a 0.5° step, is 1°. The average maximum sidelobe level obtained with the three-bit phase shifter is lower, compared to the previous case (−10.2 dB), and varies along the scanning range from −8.9 dB to −12.8 dB (which is the maximum sidelobe level in the broadside direction). The average directivity loss, calculated for

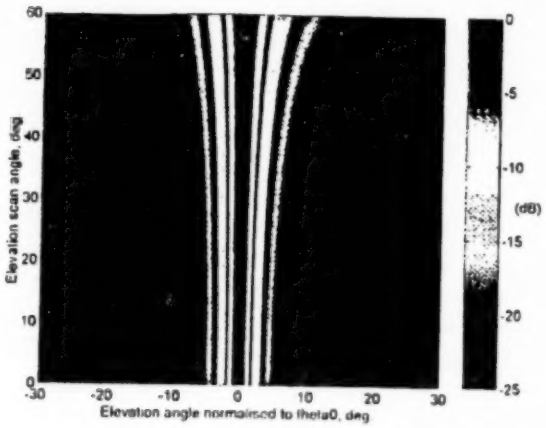

Figure 10a. The array factor of a 64-element linear array with analog five-bit phase shifters (color scale in dB).

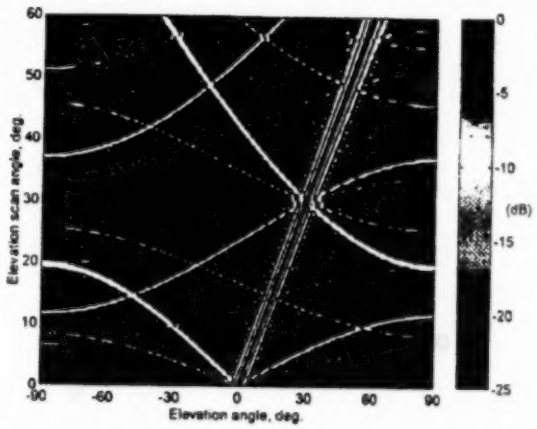

Figure 10b. The array factor of a 64-element linear array with two-bit phase shifters (color scale in dB).

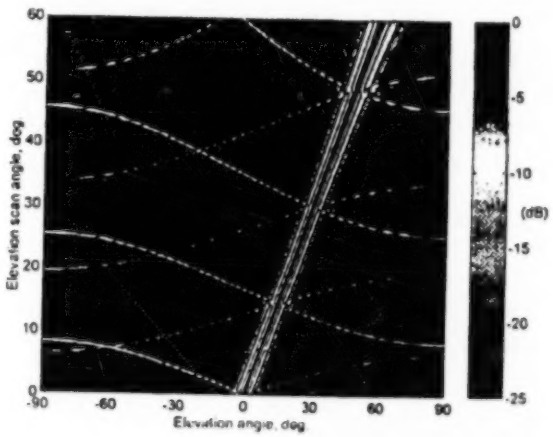

Figure 10c. The array factor of a 64-element linear array with three-bit phase shifters (color scale in dB).

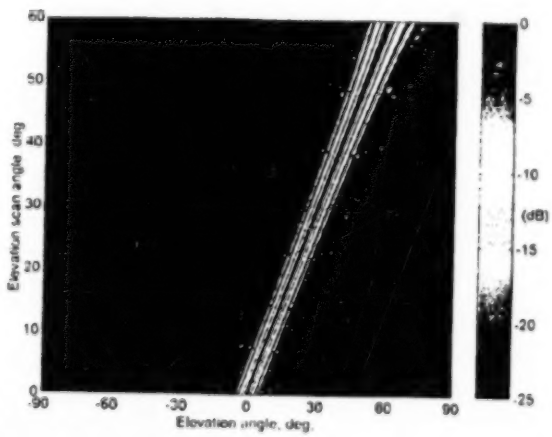

Figure 10d. The array factor of a 64-element linear array with four-bit phase shifters (color scale in dB).

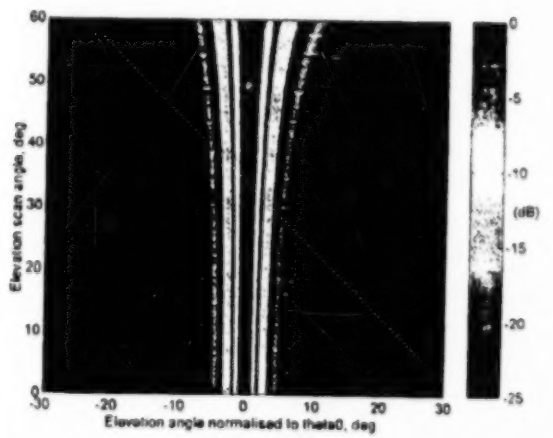

Figure 10e. The array factor of a 64-element linear array with five-bit phase shifters (color scale in dB).

$0° \le \theta_0 < 60°$ with a 0.5° step, is 0.20 dB, with a 0.42 dB peak for $\theta_0 = 14.5°$.

Note that there is no scan-angle deviation and no directivity loss for $\theta_0 = 30°$. In this case, the phase distribution obtained corresponds to the theoretical distribution, as the required phase for each element is a multiple of available phase states, i.e.,

$$kd\sin(\theta_0) = \pi/2. \quad (1)$$

where k is the wave number, d is the inter-element spacing, and θ_0 is the scan angle.

3.2.4 Four-Bit Phase Shifter

Sixteen phase states are possible with a four-bit phase shifter, starting at 0° with a 22.5° step. The maximum deviation of the phase of each element is now 11.25°. Figure 8 shows the array factor in the two-dimensional color representation.

The phase distributions are now changing more rapidly with the scan angle, following the theoretical pattern with less discrepancy. The maximum scan-angle deviation occurs for $\theta_0 = 60°$ (1.66°), and the average scan-angle deviation, calculated for $0° \le \theta_0 < 60°$ with a 0.5° step, is 0.46°. The highest sidelobe level equals −10.5 dB, and is reached around several scan angles (20°, 40°, 45°, and 60°). The average directivity loss calculated for $0° \le \theta_0 < 60°$ with a 0.5° step is lower than 0.05 dB, with a maximum of 0.1 dB occurring at 22°. Again, with this array configuration ($d/\lambda = 0.5$, where λ is the wavelength), ideal phase for the eight antenna elements can be obtained for $\theta_0 = 30°$, and neither scan-angle deviation nor directivity loss occur.

3.2.5 Five-Bit Phase Shifter

Thirty-two phase states can be now used to steer the main beam. The maximum error of the phase required for each element is then 5.625°. This considerably reduces the scan-angle deviation, as shown in Figure 9.

The average scan-angle deviation calculated for $0° \le \theta_0 < 60°$ with a 0.5° step is 0.23°, with a peak of 1° for $\theta_0 = 54.5°$. The highest sidelobe level equals −11.6 dB, occurring for 6.5° and 60°. The directivity loss is now negligible, with an average of 0.01 dB over the scanning range considered.

3.2.6 Concluding Remarks

Table 2 summarizes the average array-factor characteristics for an eight-element array utilizing one- to five-bit phase shifters. Using a four-bit phase shifter seems a good tradeoff, as the directivity loss drops to 0.05 dB, and the scan-angle deviation relative to the HPBW is only 2.9%. For this specific case, the average maximum sidelobe level is acceptable (−11.6 dB).

The array-factor characteristics of an eight-element linear phased array with a half-wavelength inter-element spacing have been fully described, considering differing numbers of bits for the phase shifter. However, an eight-element array is a relatively small array, and general analytic equations describing the characteristics of a large array cannot be applied. Thus, the study of a 64-element phased array is presented hereafter, in order to extend and generalize the different comments, and to compare our results to the theoretical results.

Table 2. The average results of scan-angle deviation, maximum sidelobe level (SLL) and directivity loss over scan angle for an eight-element linear array using phase shifters of different numbers of bits.

	Number of Phase-Shifter Bits				
	1 Bit	2 Bits	3 Bits	4 Bits	5 Bits
Scan-angle deviation, $\Delta\theta$ (deg.)	2.95	1.76	0.98	0.46	0.23
$\Delta\theta$ / HPBW (%)	18.89	11.34	5.98	2.87	1.42
Maximum SLL (dB)	−6.89	−6.97	−10.19	−11.62	−12.18
Directivity loss (dB)	3.15	0.82	0.20	0.047	0.012

The average was realized by considering a scan angle varying from 0° to 60° with a 0.5° step. The theoretical maximum sidelobe level is −12.8 dB.

3.3. 64-Element Array

The results of a 64-element linear array with a half-wavelength inter-element spacing are presented in this section. The graphs corresponding to an array utilizing analog phase shifters and two- to five-bit phase shifters are shown in Figure 10.

Figure 10a differs from the previous array-factor representation in a two-dimensional color representation as the horizontal axis is now the elevation angle, normalized to the steering angle, θ_0, i.e. only the pattern in a 60° beamwidth around the scanning direction is shown. This representation helps to visualize the principal array-factor characteristics as the HPBW becomes narrower with the increase in the number of array elements, and as the high sidelobes are closer to the main beam. Figure 10e shows a similar representation. This is not the case for the other graphs in Figure 10, because the useful information to be shown is located not only around the main beam.

The array factor of the array with two-bit phase shifters is depicted in a two-dimensional color representation in Figure 10b. Some curves appear with a mean level of about −10 dB, shown as yellow curves. The curve starts at ($\theta = 0°$, $\theta_0 = 0°$), travels in an arc to the ($\theta = -90°$, $\theta_0 = 20°$) coordinate, and then from ($\theta = 90°$, $\theta_0 = 20°$) to ($\theta = -36°$, $\theta_0 = 60°$). Other curves are visible in light green and light blue, showing lobes with lower magnitude. These curves are due to quantization lobes (QLs), which occur at specific positions depending on the scan angle, the number of array elements, and the number of bits of the phase shifter [6]. The quantization lobes can be evaluated in position and magnitude [3] if the number of array elements is at least twice the number of phase states, i.e.,

$$N \ge 2^{M+1}, \quad (2)$$

where N is the number of elements of the array, and M is the number of bits.

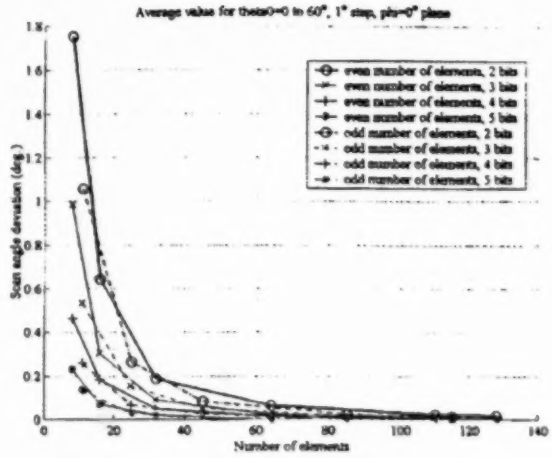
Average value for theta0=0 to 60°, 1° step, phi=0° plane
even number of elements, 2 bits
even number of elements, 3 bits
even number of elements, 4 bits
even number of elements, 5 bits
odd number of elements, 2 bits
odd number of elements, 3 bits
odd number of elements, 4 bits
odd number of elements, 5 bits
Scan angle deviation (deg.)
Number of elements

Figure 11a. The average scan-angle deviation as a function of the number of array elements.

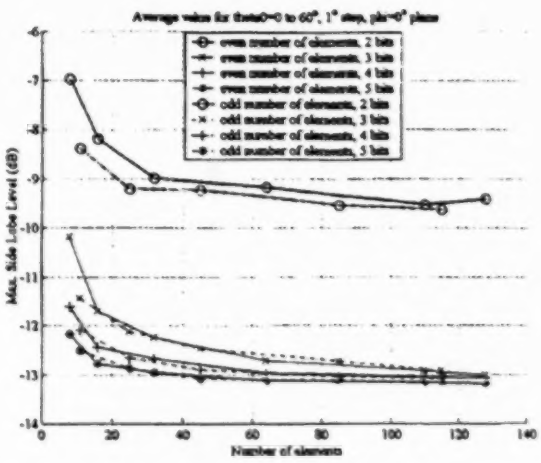
Average value for theta0=0 to 60°, 1° step, phi=0° plane
even number of elements, 2 bits
even number of elements, 3 bits
even number of elements, 4 bits
even number of elements, 5 bits
odd number of elements, 2 bits
odd number of elements, 3 bits
odd number of elements, 4 bits
odd number of elements, 5 bits
Max. Side Lobe Level (dB)
Number of elements

Figure 11b. The average sidelobe level as a function of the number of array elements.

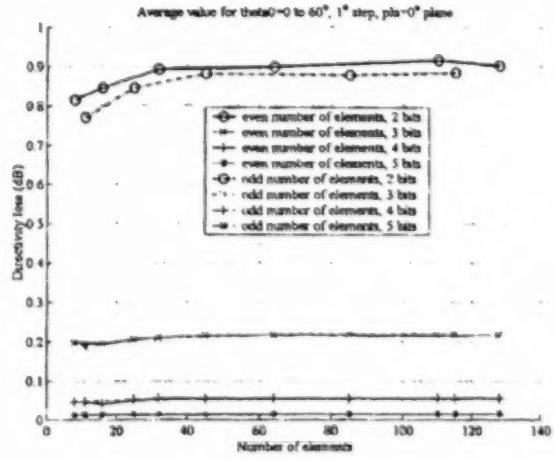
Average value for theta0=0 to 60°, 1° step, phi=0° plane
even number of elements, 2 bits
even number of elements, 3 bits
even number of elements, 4 bits
even number of elements, 5 bits
odd number of elements, 2 bits
odd number of elements, 3 bits
odd number of elements, 4 bits
odd number of elements, 5 bits
Directivity loss (dB)
Number of elements

Figure 11c. The average directivity loss as a function of the number of array elements.

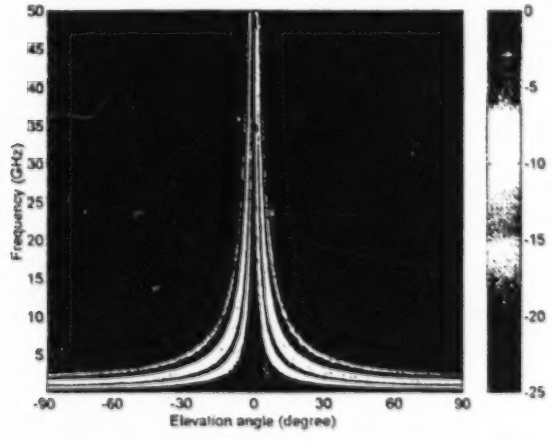

Figure 13a. A two-dimensional color plot of the array factor as a function of frequency of a 64-element linear array, pointing in the broadside direction, in the Cartesian coordinate system.

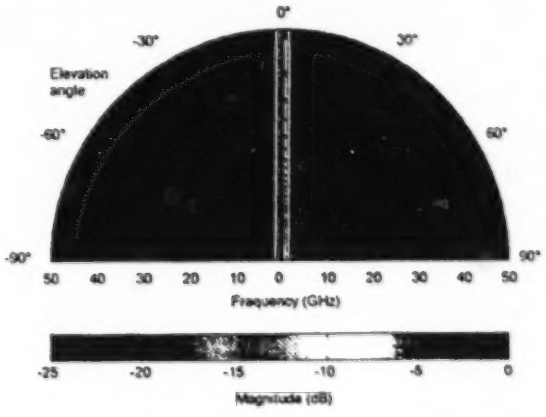

Figure 13b. A two-dimensional color plot of the array factor as a function of frequency of a 64-element linear array, pointing in the broadside direction, in the polar coordinate system.

In this case, each phase step of the discrete phase distribution modifies at least the phase of two consecutive elements, and quantization lobes will be produced as in a subarray situation [3]. In fact, quantization lobes can be considered to be grating lobes produced by arraying subarrays of two or more elements with a spacing larger than a half wavelength. For a uniformly illuminated array, the scan-angle deviation, normalized to the array beamwidth, is [7]

$$\Delta\theta_0 = \frac{\pi}{4}\frac{1}{2^M}. \tag{3}$$

The magnitude of the first quantization lobe as a function of the number of bits is shown in Table 3 (after [8]).

The yellow color of the curve indicates a −10.5 dB level, as mentioned in Table 3. The positions of the quantization lobes are the same as those of the 25-element array with the two-bit phase shifter [9]. The curves representing the higher quantization lobes are also visible, particularly the second quantization lobe, with a −14.9 dB level (light green curves).

The quantization lobes reduce the directivity, and the directivity loss can be approximated with [10]

$$Loss \cong \sin c^2\left(\frac{\pi}{2^M}\right). \tag{4}$$

The results of directivity loss as a function of the number of bits are given in Table 4 (after [8]).

When the number of array elements is less than the number of phase steps, the discrete phase distribution has a random character. The average sidelobe level due to the quantization error is given as [7, 11]

$$\sigma^2 = \frac{\pi^2}{3\times 2^{2M}}, \tag{5}$$

and the RMS sidelobe level is σ^2/N. The directivity loss generated by the increased sidelobe level is, to a first approximation, [3]

$$Loss \cong 1-\sigma^2. \tag{6}$$

The directivity loss due to random phase errors is reported for different numbers of bits in Table 4. One can notice that the directivity losses obtained with an eight-element linear array (see Table 2) are in the same order. However, the quantization lobes are not so visible on the two-dimensional color representation graphs, because the number of phase distributions is too small.

The quantization lobes also appear clearly in Figure 10c, showing the array factor of the 64-element array with three-bit phase shifters. In the range $0° \le \theta_0 \le 60°$, the first quantization lobe scans the half space more than three times. The same comment can be made about Figure 10d, depicting the array factor of the 64-element array with four-bit phase shifters. The curves are thin and dashed and almost invisible, indicating a vanishing effect of the phase quantization with the increase in the number of the phase-shifter bits. With the five-bit phase shifters, the quantization lobes are hardly discernible, due to the 25 dB color scale. The representation with the elevation angle normalized to the scan angle for the horizontal axis is then preferred. In the scanning range considered, the difference between the use of analog phase shifters and five-bit phase shifters is small. In the latter case, the quantization lobes are merged with the sidelobes, and the combination of the number of array elements and the number of bits gives a number of phase distributions high enough to obtain a scan-angle deviation lower than 0.02° over the total scanning range considered.

Table 3. The magnitude of the first quantization lobe (QL) (after [8]).

Number of Phase-Shifter Bits	QL (dB)
2	−10.5
3	−17.1
4	−23.6
5	−29.8
6	−36.0

Table 4. The directivity loss due to quantization lobes (after [8]).

Number of Phase-Shifter Bits	Regular Loss (dB)	Random Loss (dB)
2	0.912	1.000
3	0.224	0.229
4	0.056	0.056
5	0.014	0.014

Table 5. The average results of scan-angle deviation, maximum sidelobe level (SLL), and directivity loss over scan angle for a 64-element linear array for two- to five-bit phase shifters.

	Number of Phase-Shifter Bits			
	2 Bits	3 Bits	4 Bits	5 Bits
Scan angle deviation, Δθ (deg.)	0.064	0.020	0.014	0
$\Delta\theta$ / HPBW (%)	3.28	1.01	0.73	0
Maximum SLL (dB)	−9.18	−12.72	−12.97	−13.13
Directivity loss (dB)	0.90	0.22	0.054	0.013

The average was realized by considering a scan angle varying from 0° to 60° with a 1° step. The theoretical maximum sidelobe level is −13.26 dB.

Table 5 summarizes the average results of scan-angle deviation, directivity loss, and maximum sidelobe level for the 64-element linear array with different phase shifters. As mentioned with the smaller arrays, the overall characteristics are improved with the increase in the number of bits. For this specific array, note that the average scan-angle deviation, normalized to the HPBW, equals 1% for three bits. The average maximum sidelobe level stays under −12.5 dB from three bits as well. The average directivity losses drop below 0.1 dB from four bits.

The array-factor characteristics of two different arrays with digital phase shifters have been detailed and analyzed in these subsections. They have shown how characteristics such as steering angle, sidelobe level, and directivity are affected by the number of the phase-shifter bits. In order to generalize the discrepancy of the array-factor characteristics compared to the ideal case versus the number of bits, the results of arrays of other sizes, from 11 to 128 elements, are presented hereafter.

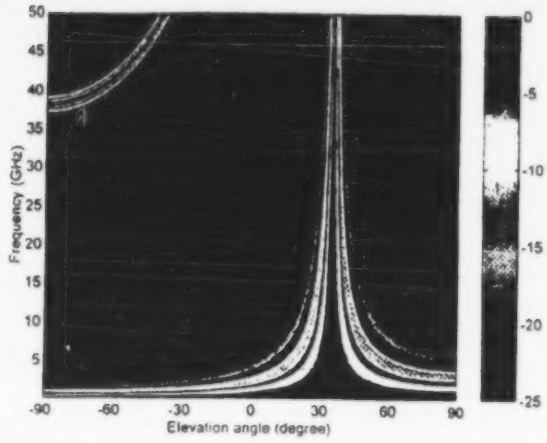

Figure 14a. A two-dimensional color plot of the array factor as a function of frequency of a 64-element linear array, with a feed system using true-time-delay lines, pointing in the $\theta_0 = 35°$ direction, in the Cartesian coordinate system.

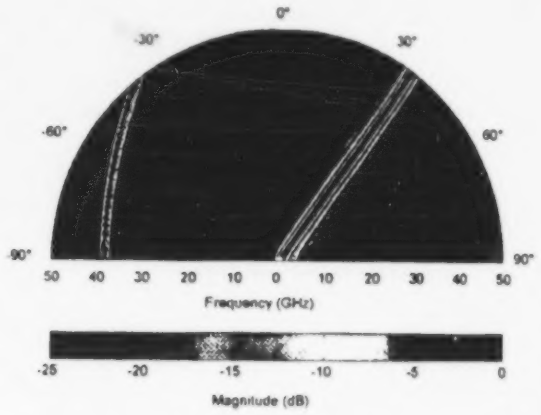

Figure 14b. A two-dimensional color plot of the array factor as a function of frequency of a 64-element linear array, with a feed system using true-time-delay lines, pointing in the $\theta_0 = 35°$ direction in the polar coordinate system.

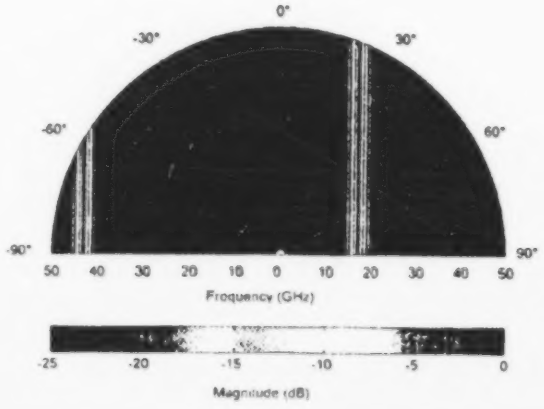

Figure 15a. A two-dimensional color polar plot of the array factor as a function of frequency of a 64-element linear array, with analog constant-phase phase shifters, pointing in the direction $\theta_0 = 35°$ at $f_0 = 30$GHz.

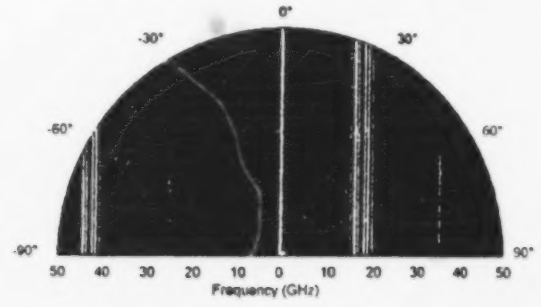

Figure 15b. A two-dimensional color polar plot of the array factor as a function of frequency of a 64-element linear array, with three-bit digital constant-phase phase shifters, pointing in the direction $\theta_0 = 35°$ at $f_0 = 30$GHz.

3.4. Arrays of Other Sizes

In this section, the array-factor characteristics, such as steering angle, maximum sidelobe level, and directivity losses, of arrays of 11, 32, 45, 85, 110, 115, and 128 elements, are presented. The graphs in Figure 11 summarize the results as a function of the number of array elements, with the number of bits as a parameter. The cases with arrays of odd and even numbers of elements are separated, as the obtained results differ somewhat.

The scan-angle deviation is plotted as a function of the number of elements of the array, with the number of the phase-shifter bits as a parameter, in Figure 11a. As shown in the previous section, the scan-angle deviation decreases with the increase in the number of bits, which causes an increase in the number of possible phase distributions. For a given number of bits, the scan-angle deviation also decreases with an increase in the number of elements, and also as the number of possible phase distributions for the array increases. Looking at the curves for arrays with odd and even numbers of elements, it appears that their behavior is linear, i.e., for the same number of bits, the curves with odd and even numbers of elements can be merged into a single continuous curve.

The maximum sidelobe level, averaged over the range $0° \le \theta_0 \le 60°$ with a 1° step, as a function of the number of elements, is shown in Figure 11b, with the number of bits as a parameter. The curves converge toward an absolute value corresponding to the maximum sidelobe level of an infinite array with an analog phase shifter (–13.26 dB). The slopes of the curves depend on the number of bits. For two bits, the slope is low, and convergence will apparently be achieved for very large arrays. The –12 dB maximum sidelobe level is obtained with only three bits from arrays larger than 20 elements, while the –13 dB level is reached with four bits for arrays larger than 64 elements, and with five bits for arrays as small as 45 elements. For a given number of bits, the curves for odd and even numbers of elements can be merged, except for two bits. Arrays of odd numbers of elements have lower maximum sidelobe levels over the scanning range considered, but the difference is only about 0.2 dB. However, arrays with a two-bit phase shifter have an average maximum sidelobe level higher than –10 dB, which is an unacceptable value for most applications.

The difference between arrays of odd and even numbers of elements with a two-bit phase shifter is reflected in the directivity losses, as shown in Figure 11c, even though the difference is only 0.02 dB. As we can see, the directivity loss depends essentially on the number of bits of the phase shifter, even for small arrays. The mean (in terms of array size) directivity losses, averaged over a scanning range from $0 \le \theta_0 \le 60°$ with a 1° step, are about 0.89 dB, 0.22 dB, 0.0535 dB, and 0.013 dB for two, three, four, and five bits, respectively. These results are in good agreement with the theoretical values given in Table 4.

To summarize the results presented in this section, a phase shifter with three or four bits gives adequate array-factor characteristics for most of the applications. For small arrays, the use of four-bit or even five-bit phase shifters is preferred because of the reduced number of phase distributions due to the small number of elements, while the use of three-bit or even two-bit phase shifters is sufficient for arrays larger than 32 elements.

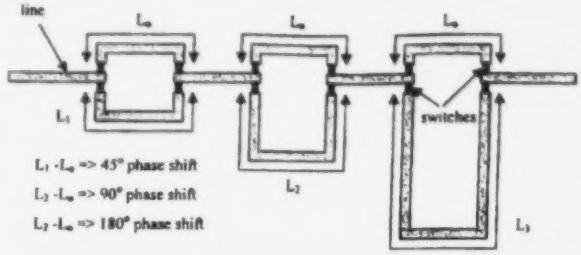

Figure 12. A three-bit switched-line phase shifter.

4. Array Factor as a Function of Frequency

In this section, the variations of the array factor with frequency are investigated. For this study, a 64-element array with a half-wavelength inter-element spacing at 30 GHz is considered. At 30 GHz, a half wavelength is 1.0 cm, which is left unchanged when the array performance is calculated at other frequencies. Results of arrays with constant-phase phase shifters and switched-line phase shifters are compared to those of an array with true-time-delay lines. Finally, results of an array combining phase shifters and true-time-delay units at the subarray level are presented. The phase weighting applied to each element is defined at 30 GHz. The frequency range of interest is 1 to 50 GHz.

Each antenna element in the array can be fed through a phase shifter, which allows the array beam to scan. Different kinds of phase shifters can be considered. The first kind is based on a constant-phase concept. The phase for each element is determined at a specific frequency, and remains constant over the frequency range of interest. If the phase shifter is digital, the chosen phase is the closest one of the possible phase states (see Figure 4). The second kind of phase shifter is based on a switched-line concept, and is directly related to MMIC (microwave monolithic integrated circuit) technology, which uses switches and lines of different lengths to obtain a set of phase steps. For example, a three-bit switched-line phase shifter is shown in Figure 12.

In the case of switched lines, the phase, φ_n, delivered to the nth element is expressed by

$$\varphi_n = 2\pi f \tau_n, \quad \text{with} \quad \tau_n = \frac{L_n}{c}, \tag{7}$$

where τ_n is the delay for the nth element, L_n is the length of the delay line selected for the nth element, f is the frequency, and c is the speed of light.

Considering the example presented in Figure 12, the phase delivered to the nth element corresponds to the total length $L_n = b_1(L_1 - L_0) + b_2(L_2 - L_0) + b_3(L_3 - L_0)$, where b_i is 0 or 1. Note that the maximum length of the line is a full wavelength at the frequency under consideration. The required phase is then modulus 2π.

Another method to steer the main beam is also considered, based on the use of true time-delay (TTD) lines for each element.

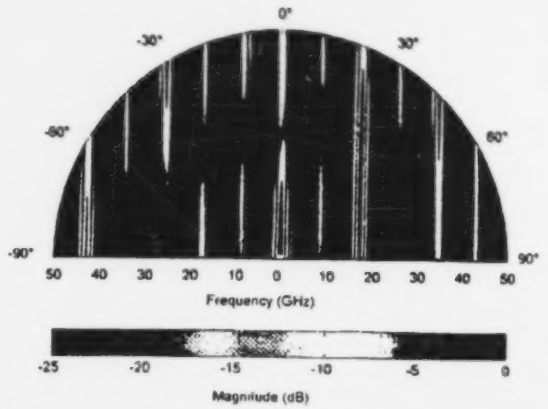

Figure 16a. A two-dimensional color polar plot of the array factor as a function of frequency of a 64-element linear array with three-bit switched-line phase shifters, pointing in the direction $\theta_0 = 35°$ at $f_0 = 30\text{GHz}$, with the phase weightings evaluated at 30 GHz.

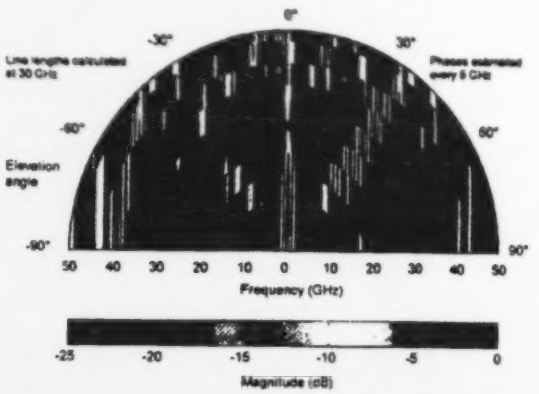

Figure 16b. A two-dimensional color polar plot of the array factor as a function of frequency of a 64-element linear array with three-bit switched-line phase shifters, pointing in the direction $\theta_0 = 35°$ at $f_0 = 30\text{GHz}$, with the phase weightings re-instantiated every 5 GHz.

Figure 18a. A two-dimensional color polar plot of the array factor as a function of frequency of a 64-element linear array with three-bit switched-line phase shifters and true-time-delay units associated with 16-element subarrays, pointing in the direction $\theta_0 = 35°$ at $f_0 = 30\text{GHz}$.

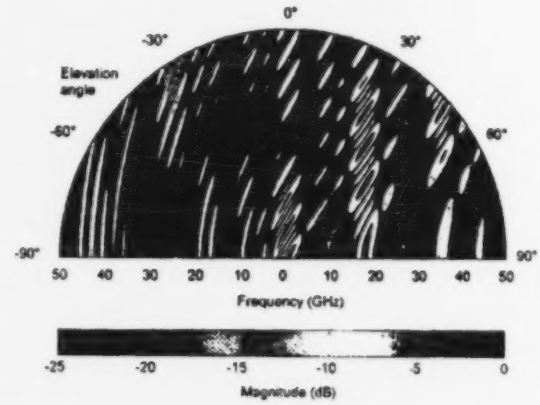

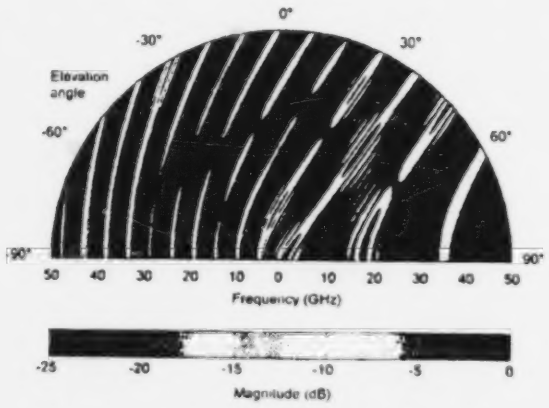

Figure 18b. A two-dimensional color polar plot of the array factor as a function of frequency of a 64-element linear array with three-bit switched-line phase shifters and true-time-delay units associated with eight-element subarrays, pointing in the direction $\theta_0 = 35°$ at $f_0 = 30\text{GHz}$.

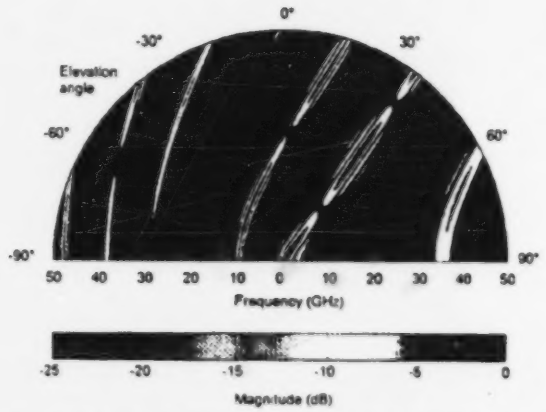

Figure 18c. A two-dimensional color polar plot of the array factor as a function of frequency of a 64-element linear array with three-bit switched-line phase shifters and true-time-delay units associated with four-element subarrays, pointing in the direction $\theta_0 = 35°$ at $f_0 = 30\text{GHz}$.

In this case, the length of the line required for the nth element, expressed by Equation (8), is such that the corresponding phase is exactly the phase required to scan in the desired direction. In other words, the phase is not restricted to the interval $[0, 2\pi]$. Thus,

$$L_n = nd\sin(\theta_0), \tag{8}$$

where d is the inter-element spacing, and θ_0 is the scan angle.

Before introducing the results for a 35° scan angle, the two-dimensional color plot of the array factor of a 64-element array, pointing in the broadside direction, is depicted in Figure 13. For comparison, Figure 13a shows the array factor as a function of frequency in the Cartesian coordinate system, whereas Figure 13b shows it in the polar coordinate system. In the former, the decrease of the HPBW with frequency is well visible, and represents the main feature of this graph. In the latter, the color curves representing the main lobe (red curve) and the sidelobes (light blue and green curves) are straight lines, although the plot is in the polar coordinate system. This representation is then considered throughout this section.

Since the lengths of the delay lines are the same for each element, the particular array factor corresponds to the array factor of an array with uniform phase and amplitude distributions. Therefore, the array factor (AF) is expressed by

$$AF(\theta) = \frac{\sin\left[N\pi\frac{d}{\lambda}\sin(\theta)\right]}{N\sin\left[\pi\frac{d}{\lambda}\sin(\theta)\right]}, \tag{9}$$

where N is the number of array elements, d is the inter-element spacing, λ is the wavelength, and θ is the elevation angle as defined in Figure 2.

The positions of the minima and grating lobes, for instance, are given by Equation (10), which is the equation of a straight line in the polar coordinate system (see the Appendix) [12]:

$$N\pi\frac{d}{\lambda}\sin(\theta_p) = p\pi, \tag{10}$$

or

$$\sin(\theta_p) = \frac{p}{Nd}\frac{c}{f}, \tag{11}$$

where p is an integer, c is the speed of light, f is the frequency, θ_p is the pth minima or grating lobe. With the same array configuration, the array factor with a scan angle θ_0 is expressed by

$$AF(\theta) = \frac{\sin\left\{N\pi\frac{d}{\lambda}\left[\sin(\theta)-\sin(\theta_0)\right]\right\}}{N\sin\left\{\pi\frac{d}{\lambda}\left[\sin(\theta)-\sin(\theta_0)\right]\right\}}. \tag{12}$$

The scan angle is given by Equation (8), with $n = 1$. This equation reduces to $L_0 = d\sin(\theta_0)$, and L_0 represents the length of the elementary true-time-delay line.

Considering a scan angle of θ_0, the positions of the minima and grating lobes are given by

$$N\pi\frac{d}{\lambda}\left[\sin(\theta_p)-\sin(\theta_0)\right] = p\pi \tag{13}$$

or

$$f = \frac{p}{Nd\sin(\theta_0)}\frac{c}{\frac{\sin(\theta_p)}{\sin(\theta_0)}-1}. \tag{14}$$

Since $1/\sin(\theta_0) > 1$, the equation corresponds to that of a hyperbola (see the Appendix) [12]. This is illustrated in Figure 14, where the array factor of a 64-element array with a true-time-delay unit per element, pointing in the 35° direction, is plotted in the two-dimensional color graph.

The grating lobe (GL) appears clearly on the left side of the plot, for frequencies above 38 GHz. The grating lobe occurs when

$$\frac{d}{\lambda} = \frac{1}{\left[\sin(\theta_g)-\sin(\theta_0)\right]}, \tag{15}$$

where θ_g is the position the grating-lobe maximum. In the case considered, the inter-element spacing is a half-wavelength at $f_0 = 30$ GHz, and the scanning angle, θ_0, is 35°. The above equation becomes

$$f = \frac{2f_0}{\sin(\theta_0)}\frac{1}{1-\frac{\sin(\theta_g)}{\sin(\theta_0)}}. \tag{16}$$

The first grating lobe occurs at –90° for 38.1 GHz, and at –38.8° for 50 GHz. Note that Equation (16) corresponds to the equation of a hyperbola.

4.1. Arrays with Constant-Phase Phase Shifters

A 64-element array with a half-wavelength spacing and with constant phase shifters is now investigated. We consider first an analog constant-phase phase shifter, i.e., the phase weighting the nth antenna element at the frequency f_0 is exactly the required phase to steer in the θ_0 direction, or

$$\varphi_n = n\varphi_0 \tag{17a}$$

with

$$\varphi_0 = \frac{2\pi}{\lambda_0}d\sin(\theta_0), \tag{17b}$$

where λ_0 is the wavelength at f_0. The phase weightings remain constant with frequency. The array factor is then expressed by

$$AF(\theta) = \frac{\sin\left\{N\pi\frac{d}{\lambda}\left[\sin(\theta)-\frac{\varphi_0}{2}\right]\right\}}{N\sin\left\{\pi\frac{d}{\lambda}\left[\sin(\theta)-\frac{\varphi_0}{2}\right]\right\}}. \tag{18}$$

The positions of the minima and grating lobes are given by

$$N\pi\frac{d}{\lambda}\left[\sin(\theta_p)-\frac{\varphi_0}{2}\right]=p\pi, \tag{19}$$

or

$$\sin(\theta_p)=\frac{\left(p\pi+\frac{\varphi_0}{2}\right)}{N\pi d}\frac{c}{f}. \tag{20}$$

This expression is the equation of a straight line in the polar coordinate system (see the Appendix), and can be seen in the corresponding two-dimensional color plot depicted in Figure 15a.

Figure 15a also shows the grating lobe, which occurs at 42 GHz and above. The frequency where the grating lobe appears can be determined using Equation (15), where θ_0 is now varying with frequency. The expression of the scan angle as a function of frequency, $\theta_0(f)$, is

$$\sin[\theta_0(f)]=\frac{f}{f_0}\sin[\theta_0(f_0)]. \tag{21}$$

The above equation is simply obtained by equating the denominator of the array factor given in Equation (18) to zero, which also determines the position of the array-factor maximum.

The two-dimensional color plot of a 64-element array with a half-wavelength inter-element spacing, fed through three-bit constant-phase phase shifters, is presented in Figure 15b. The graph is similar to the previous graph. Because the phase shifter is digital, quantization lobes occur, and their variation as a function of frequency implies additional straight lines. Note also that for this array and this configuration, the sidelobe levels on each side of the main beam are not symmetric, and the sidelobes on the right side have higher magnitude.

4.2. Arrays with Switched-Line Phase Shifters

The two-dimensional color plot of a 64-element array with a half-wavelength inter-element spacing, with a three-bit switched-line phase shifter, is presented in Figure 16a. This figure shows first that the main lobe is not pointing in the desired direction when the frequency varies from the designed frequency, f_0 ($f_0 = 30$ GHz). It also shows that array factors with only one lobe with high level (0 dB or so) appear in a small frequency range around f_0, called hereafter the clear zone of the frequency range. The variations of the high-level-lobe positions as a function of frequency are straight lines with a fluctuating level. In particular, a high-level lobe occurs in the broadside direction. The magnitude is 0 dB at low frequencies, and it decreases until the lobe vanishes below −25 dB throughout the clear zone of the frequency range. Finally, this lobe appears again with a significant level at higher frequencies. Note that the grating lobe occurs first at −90° for a frequency higher than the case of the array fed through true-time-delay (TTD) units (about 42 GHz), as the scan angle obtained is smaller than the expected scan angle.

If the array is used for a narrowband signal around a center frequency in different bands, then the phase weightings can be re-

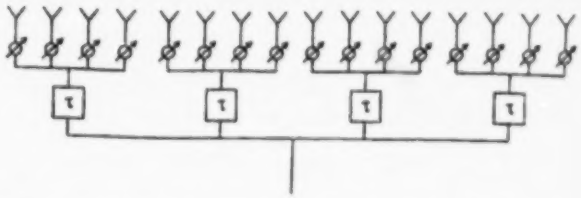

Figure 17. A phased array with phase shifters and true-time-delay units.

instantiated to keep the main beam in the desired direction. Figure 16b shows an example when the phase weightings are calculated every 5 GHz. In this case, the squint of the main-beam peak is considerably reduced. However, at low frequencies, the main lobe occurs in the broadside direction, as the length of the switched lines are too short compared to the wavelength to deliver the required phase weightings.

4.3. Arrays with True-Time-Delay (TTD) Units and Switched-Line Phase Shifters

To avoid the beam squint due to wide-frequency-band operation with a large array, a common approach is to associate phase shifters for each element with true-time-delay units at the subarray level [3, p. 188; 6, p. 511], as indicated in Figure 17. Using a combination of these two devices is a tradeoff among scanning performance, size, and the cost of the system.

In the present case, three-bit switched-line phase shifters are used. The phase shifters are designed to operate at 30 GHz. The lengths of the true-time delay units are such that each true-time-delay unit produces the required phase at the center of the subarray to steer the main beam in the desired direction (here, 35°). Therefore, the true-time-delay units have different lengths.

Figure 18 depicts the results of array factors as a function of frequency for 64-element arrays with a three-bit switched-line phase shifter for each element, and a true-time-delay unit for a subarray of 16, eight, and four elements, respectively. Comparing Figure 18a to Figure 16a – which corresponds to a 64-element array with a three-bit switched-line phase shifter for each element and without true-time-delay units – one can see that the straight red line representing the main beam on the latter is segmented in the former. Each segment is tilted, due to the effect of the true-time-delay units. The centers of the segments remain almost on the straight line. The same remark can be made for the lines representing the two main grating lobes. Some secondary lobes appear on each side of the segments, especially in the $\theta = 35°$ direction. With this array configuration, the array beam scans in the desired direction over a sub-frequency band. This behavior is emphasized in Figure 18b, which represents the array factor of a 64-element array with the previous configuration, but with a true-time-delay unit for eight elements. On this plot, the number of hyperbolas representing the grating lobes over frequency decreases. The red segment representing the main lobe, centered around 30 GHz in the $\theta = 35°$ direction, is longer, indicating a larger operating frequency band. Aside from the 30 GHz sub-band, the radiated power is divided mainly into two beams. Figure 18c shows the radiation patterns of a 64-element array with the previous configuration, but with a true-time-delay unit for four elements. The number of grating lobes decreases. As the number of true-time-delay units increases, the two-dimensional color plot of the array factor as a

function of frequency tends logically towards the plot corresponding to a phased array with true-time-delay units for each element (see Figure 14).

These figures show that the main beam is following the desired direction over the frequency range if the number of true-time-delay units is important enough. However, the main-lobe level vanishes for some frequencies, and sidelobes then become dominant. The additional high-level lobes are due to grating lobes generated by the subarray arrangement of the elements. Detailed information can be found in [8].

The use of true-time-delay lines in the feed network gives the best results, keeping the scan angle constant over the frequency range. The use of both phase shifters introduces a frequency dependence on the scan angle, which is clearly visible in straight color lines in the two-dimensional color polar plots. The constant-phase phase shifter is preferred, as no 0-dB-magnitude lobes other than grating lobes are added. However, the switched-line phase shifter is the more realistic phase shifter, and gives the worst results in a broadband utilization. However, using a combination of a phase shifter for each element and a true-time-delay unit at the subarray level considerably increases the operating bandwidth with a moderate cost.

5. Conclusion

This paper has presented the results of investigations on the radiation characteristics of linear arrays using feed networks with phase-shifting devices. Arrays of point-source elements, having different sizes in terms of the number of elements and inter-element spacings, have been considered. Studies of the array-factor characteristics have been carried out over specified scanning and frequency ranges.

In the first part, the impact on the radiation characteristics of changes in the number of digital phase-shifter bits have been pointed out, by detailed studies of arrays of various numbers of elements. With the help of two-dimensional color graphic representations, it has been shown qualitatively that the limited number of phase distributions across the array, due to quantization:

- generates scan-angle discrepancies depending on the number of bits and the number of array elements;
- increases sidelobe levels;
- introduces additional lobes, called quantization lobes, the levels of which depend on the number of bits;
- and, as a result of all the above, decreases the directivity.

All of these characteristics have been quantified for arrays of different sizes with phase shifters of different numbers of bits. This has helped to determine the optimum number of bits, considering a specific criterion.

Thus, for most applications, and considering the overall characteristics, three-bit digital phase shifters are sufficient for large arrays. The four-bit and even five-bit digital phase shifters are preferred for small arrays, because of the reduced number of possible phase distributions due to the small number of elements.

In the second part, the characteristics of 64-element arrays have been investigated as a function of frequency, when true-time-delay lines, constant-phase, and switched-line phase shifters (analog or digital), and a combination of a phase shifter for each element and true-time-delay units at the subarray level were considered. The different effects of frequency on the array factor have been clearly identified with the help of the two-dimensional color graphic representations, and mathematical descriptions have been provided. Best results were achieved with true-time-delay lines for each element, which maintain the scan angle as a constant over the frequency range. The two kinds of phase shifters – constant-phase and switched-line phase shifters – bring a frequency dependence to the scan angle. The latter, which is the most realistic, generates additional high-level lobes, and so it is the worst phase shifter for utilization over a broad frequency range. However, combining a phase shifter for each element and true-time-delay units at the subarray level improves performance over the bandwidth.

The two-dimensional color plot is a very interesting representation for visualizing a pattern over a range. Some characteristics can be easily and readily pointed out, compared to the conventional two-dimensional representation. This paper outlines the possibility of such a representation for use in phased-array studies. For instance, radiation-pattern characteristics of a phased array, taking into account models of realistic phase shifters, models of amplifiers, or mutual coupling, can also be investigated with this kind of graph, and reveal unexpected effects.

6. Appendix: Equations of a Line and Conics in the Polar Coordinate System

Figure 19 shows the Cartesian and polar coordinate systems used in this appendix.

6.1 Equation of a Line

The general equation of a line in the two-dimensional Cartesian coordinate system is expressed by

$$ax + by + c = 0 \tag{22}$$

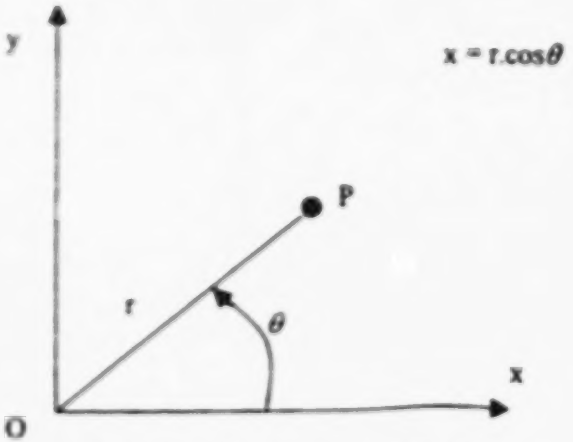

Figure 19. The Cartesian and polar coordinate systems.

Considering the Cartesian-to-polar transformation gives

$$r\cos\theta\cos\alpha + r\sin\theta\sin\alpha + r_0 = 0, \tag{23a}$$

with

$$r_0 = \frac{c}{\sqrt{a^2+b^2}}, \tag{23b}$$

or

$$r = -\frac{r_0}{\cos(\theta-\alpha)}. \tag{24}$$

6.2 Equation of Conics [12]

Conics can have different expressions, in either Cartesian or polar coordinate systems. In the polar coordinate system, the equation of the conics referred to a focus such as a pole is

$$r = \frac{p}{1+\varepsilon\cos(\theta-\alpha)}, \tag{25}$$

where ε is a positive number. Different cases occur. If $\varepsilon > 1$, the conic is a hyperbola. If $\varepsilon = 1$, the conic is a parabola. If $0 < \varepsilon < 1$, the conic is an ellipse, and if $\varepsilon = 0$, the conic is a circle.

7. References

1. R. C. Hansen, "Key Developments in Phased Arrays," *IEEE Antennas and Propagation Magazine*, **42**, 6, December 2000, pp. 110-111.

2. M. Clénet and G. A. Morin, "Graphical Investigation of Quantisation Effects of Phased Shifters on Array Patterns," Internal Report, DREO TR 2000-92, November 2000, 63 pages.

3. R. C. Hansen, *Phased Array Antennas*, New York, John Wiley and Sons, 1998.

4. P. O. Iversen, Ph. Garreau, and D. Burrell, "Real-Time Spherical Near-Field Handset Antenna Measurements," *IEEE Antennas and Propagation Magazine*, **43**, 3, June 2001, pp. 90-94.

5. R. J. Pogorzelski, "On a Simple Method of Obtaining Sidelobe Reduction over a Wide Angular Range in One and Two Dimensions," *IEEE Transactions on Antennas and Propagation*, **49**, 3, March 2001, pp. 475-482.

6. R. J. Mailloux *Phased Array Antenna Handbook*, Norwood, MA, Artech House, 1994.

7. C. J. Miller, "Minimizing the Effects of Phase Quantisation Errors in an Electronically Scanned Array," "Proc. 1964 Symp. Electronically Scanned Phased Arrays and Applications, Volume I," RADC-TDR-64-225, Griffith AFB, pp. 17-38.

8. A. W. Rudge, K. Milne, A. D. Olver, and P. Knight, *The Handbook of Antenna Design*, London, Peter Peregrinus Ltd., 1986.

9. M. Clénet and G. A. Morin, "Investigations on Radiation Characteristics of Linear Array Antennas with Digital Phase Shifters," 2001 URSI Commission B International Symposium on Electromagnetics, Victoria, BC, Canada, May 8-13, 2001, pp. 85-87.

10. J. L. Allen et al., "Phased Array Radar Studies," MIT Lincoln Lab TR 238, August 1960.

11. R. J. Mailloux, "Array Grating Lobes Due to Periodic Phase, Amplitude and Time-Delay Quantisation," *IEEE Transactions on Antennas and Propagation*, **AP-32**, 12, December 1984, pp. 1364-1368.

12. W. Gellert, H. Küster, M. Hellwich, and H. Kästner, *The VNR Concise Encyclopedia of Mathematics*, New York, Van Nostran Reinhold Company, 1977.

Introducing the Feature Article Authors

Michel Clénet was born in Nantes, France, in 1968. He received the Diplôme d'Études Approfondies (DEA) degree from the University of Rennes I, France, in 1992, and the PhD degree from the University of Nantes, France, in 1997. From 1993 to 1997, he was with the Laboratory of Electronic and Computer Systems at IRESTE, Nantes, France, where he worked on antenna systems for portable terminals. From 1997 to 1999, he was a postdoctoral fellow at the University of Manitoba, Winnipeg, Canada, where he worked on microstrip antennas, arrays, and horns, focusing on bandwidth enhancement and gain improvement. Since 1999, he has been with Defence Research and Development Canada (DRDC) Ottawa, Canada, where he has been working on planar antennas, phased arrays and related technologies, for satellite communication applications.

Gilbert A. Morin was born in Lorrainville, Canada, in 1952. He received his BScA degree in Engineering Physics from Ecole Polytechnique de Montréal, in 1977. He also received his MASc and PhD, both in Electrical Engineering, from the University of Toronto in 1980 and 1987, respectively. Since then, he has been working at Defence Research and Development Canada (DRDC) Ottawa, as a Defence Scientist in the Milsatcom Group. His research interests are millimeter-wave microcircuits, micro-electromechanical systems (MEMS), and antennas, especially phased arrays.

Defence Research and Development Canada | Recherche et développement pour la défense Canada

Canada

Français | Contact Us | Help | Search | Canada Site
Home | Defence R&D Canada | Defence Site

Top | Previous | Document: 1 of 2 | Next | Bottom | Order | Download

Browse Indexes

Titles

Authors

Descriptors

Corporate Authors

Corporate Acronyms

Document Numbers

Search Database

Summary

It is recommended you search "Authors" and "Corporate Authors" on their respective "Browse" pages.

Click here if you are having problems displaying text (ie. text is too big, or too small) or page appears to be jumbled.

TITLE: Visualization of Radiation-Pattern Characteristics of Phased Arrays using Digital **Phase Shifters**

PERSONAL AUTHOR: Clénet, M.; Morin, G.A.
CORPORATE AUTHOR: Defence R&D Canada - Ottawa, Ottawa ONT (CAN)

ABSTRACT: This article presents graphical investigations of the array factor of phased arrays with digital phase shifters. A software program, based on basic antenna array theory, has been developed in MATLAB to obtain the main array characteristics (array factor and directivity). The array factors of linear arrays of different sizes with different types of phase shifters have been studied as a function of the number of bits and the frequency. Unconventional two-dimensional color graphical representations are used to identify some characteristics of the array factor or arrays with digital phase shifters that can not be so clearly and quickly visualized with conventional graphical representations. In particular, the effects of quantization on the array factor for arrays of different sizes and for phase shifters with different numbers of bits, over scanning, and frequency, are shown using this representation. Numerous data are also provided.

REPORT NUMBER: DREO-SL-2001-102; Scientific Literature | **REPORT DATE:** 25 Aug 2004 | **NUMBER OF PAGES :** 17

Reprints: IEEE Antennas and Propagation Magazine, vol 45, no 3, 2003, p 20-35

DRDKIM N°: CA024524 | **CANDIS N°:** 522102 | **Format(s):**Hardcopy;Document Image stored on Optical Disk

Date modified: 2005-04-05

Important Notices